

## OPTICS

# Long-distance optical pulling of nanoparticle in a low index cavity using a single plane wave

E. Lee<sup>1\*</sup> and T. Luo<sup>1,2,3\*</sup>

Optical pulling force (OPF) can make a nanoparticle (NP) move against the propagation direction of the incident light. Long-distance optical pulling is highly desired for nano-object manipulation, but its realization remains challenging. We propose an NP-in-cavity structure that can be pulled by a single plane wave to travel long distances when the spherical cavity wrapping the NP has a refractive index lower than the medium. An electromagnetic multipole analysis shows that NPs made of many common materials can receive the OPF inside a lower index cavity. Using a silica-Au core-shell NP that is encapsulated by a plasmonic nanobubble, we experimentally demonstrate that a single laser can pull the Au NP-in-nanobubble structure for ~0.1 mm. These results may lead to practical applications that can use the optical pulling of NP, such as optically driven nanostructure assembly and nanoswimmers.

## INTRODUCTION

A nanoparticle (NP) facing a light trades momentum with the incoming photons and can thus get pushed to move in the light propagation direction. In some rare cases, optical pulling can be realized but is only made possible when the momentum of the incident photon along the propagation axis is smaller than the momentum of the scattered photons projected to the propagation axis (1–3). This far-field principle has guided the realization of a number of optical pulling strategies, such as using a “tractor beam” as the incident light (1–6), transmitting photons to the higher-refractive index medium from the lower one (7), and implanting photon-emitting compounds in an NP (8, 9). In practice, optical pulling can add another degree of freedom for light manipulation of nano/micro-objects and may be leveraged for biological applications (e.g., molecular assembly/sorting/sensing and drug delivery) and nanotechnologies (e.g., nanoswimmers and nanopatterning) (1–9).

However, it is still challenging to optically pull an NP in a homogeneous medium for a long distance, even practical applications usually demand so. Theoretically, a tractor beam was predicted to pull an object for ~14 cm when the object is designed to have special optical properties (e.g., transverse isotropy, antireflection coating, etc) (6), but such long-distance pulling is yet to be experimentally demonstrated. While tractor beam has been shown to pull polystyrene particles in water, the travel distances are only 10 to 20  $\mu\text{m}$  (4, 5). This short moving distance is limited by the effective range of the tractor beam, which should be nondiffractive. A single plane wave as an incident light source can potentially eliminate the pulling range problem, but the far-field principle prevents it from pulling an NP in a homogeneous medium, since a plane wave has an incident angle of zero and thus the maximum momentum along the propagation direction.

In optical pulling experiments using the tractor beam, Brzobohatý *et al.* (4) and Damková *et al.* (5) have reported that optical coupling between two microparticles can enhance the strength of pulling force. While

the enhancement remains on microsized particles under the tractor beam configuration, the result implies that a plane wave may leverage optical binding to enable optical pulling on NPs. Theoretical studies show that when an NP optically couples to a nearby object, a single plane wave can potentially pull the NP (10, 11). The far-field principle cannot intuitively explain this phenomenon because such an optical pulling force (OPF) is rooted from near-field effects. It is the interplay between different modes (e.g., electric/magnetic dipole or quadrupole) in the coupled field that enables such counterintuitive OPF. For instance, Guo *et al.* (10) proposed theoretically that a single plane wave could pull a silica NP against the photon stream when the imaginary part of the electric dipole moment of the silica NP was reversed by optically coupling to a nearby Au NP that is 50 to 100 nm away. However, the two optically coupled objects (i.e., optically binding objects) can move apart (or stick together) when the opposite optical forces on them are repulsive (or attractive) (10, 11), diminishing their optical coupling and thus OPF. As a result, such a strategy requires the optically coupled objects to stay close by to pull one of them for long distances, but it has not been demonstrated yet.

Here, we show that optical pulling using a single plane wave can be realized by using an NP-in-cavity structure (Fig. 1) if the cavity has a refractive index lower than the medium. The cavity transforms the incident single plane wave into unique internal modes that lead to OPF on the NP. We express the optical force on the NP in a simplified analytical form, which intuitively shows that the signs of the modal coefficients of the internal field determine the direction of the optical force. In the cavity, the multiplication of electric dipole-electric quadrupole (or electric dipole-magnetic dipole) coefficient has a negative sign of the real (or imaginary) part. This optical condition can lead to a negative sign of the optical force when the incident light is at the off-resonance wavelength of the NP. For example, a 300-nm air cavity in water can induce an OPF on a 100-nm Au NP using a laser with a wavelength of 600 to 1000 nm. To generate such an NP-in-cavity structure, we use a laser at the surface plasmonic resonance (SPR) peak to thermally excite Au NP to generate a vapor nanobubble to encapsulate it. We then experimentally demonstrate that a loosely focused Gaussian beam, mimicking the plane wave, can pull such an Au NP to move for a long distance of ~120  $\mu\text{m}$  when the NP is encapsulated by the plasmonic nanobubble, which

Copyright © 2020  
The Authors, some  
rights reserved;  
exclusive licensee  
American Association  
for the Advancement  
of Science. No claim to  
original U.S. Government  
Works. Distributed  
under a Creative  
Commons Attribution  
NonCommercial  
License 4.0 (CC BY-NC).

<sup>1</sup>Department of Aerospace and Mechanical Engineering, University of Notre Dame, Notre Dame, IN, USA. <sup>2</sup>Department of Chemical and Biomolecular Engineering, University of Notre Dame, Notre Dame, IN, USA. <sup>3</sup>Center for Sustainable Energy of Notre Dame (ND Energy), University of Notre Dame, Notre Dame, IN, USA.

\*Corresponding author. Email: elee18@nd.edu (E.L.); tluo@nd.edu (T.L.)

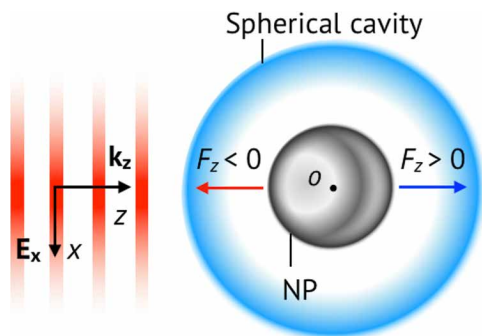


**Fig. 1. Schematic of the optical configuration of an NP-in-cavity structure facing a linearly polarized plane wave.**  $\mathbf{k}_z$  is the wave vector,  $\mathbf{E}_x$  is the electric field, and  $F_z$  depicts the optical force on the NP. The NP and the cavity are co-centered at the origin ( $\mathbf{O}$ ) of the coordinate.

acts as a lower index cavity in the liquid water medium. The key to the realized long-distance optical pulling is that the intensely excited Au NP at its SPR can keep vaporizing water where ever it moves, effectively “brining” the optically coupling cavity with it.

## RESULTS AND DISCUSSION

We first theoretically study a scenario where a single plane wave is incident on a spherical cavity that encapsulates an NP. To simplify the mathematics, but without the loss of generality, we consider that the NP and the cavity are co-centered, the incident electric field is polarized in the  $x$  direction, and it propagates along the  $z$  direction (see Fig. 1). In this system, the NP experiences an optical force ( $F_z$ ) in the  $z$  direction, which is approximated as (see text S1 for details)

$$F_z \cong (F_{ee} + F_{mm} + F_{em}), \begin{cases} F_{ee} = \left(\frac{\pi\epsilon_0}{k_0^2}\right) \frac{12}{5} \mathbf{Im}(e_d e_q^* S_{ee}), \\ F_{mm} = \left(\frac{\pi\epsilon_0}{k_0^2}\right) \frac{12}{5} \mathbf{Im}(m_d m_q^* S_{mm}), \\ F_{em} = \left(\frac{\pi\epsilon_0}{k_0^2}\right) \frac{4}{3} \mathbf{Im}(e_d m_d^* S_{em}) \end{cases} \quad (1)$$

where  $F_{ee}$  (or  $F_{mm}$ ) is the electric (or magnetic) dipole-quadrupole interaction component,  $F_{em}$  is the electric dipole-magnetic dipole interaction component, and  $e_d$  (or  $m_d$ ) and  $e_q$  (or  $m_q$ ) represent, respectively, the complex amplitudes of electric (or magnetic) dipole and quadrupole modes of the incoming light to the NP. With the first-order scattering approximation (i.e., the reflected lights from the NP toward the cavity are ignored), the incoming light becomes the internal field of the cavity that is without the NP. Thus, the multipole coefficients ( $e_d$ ,  $e_q$ ,  $m_d$ , and  $m_q$ ) solely depend on the size factor ( $\gamma_c = k_0 n_m r_c$ ) and the refractive index ratio ( $m_c = n_c/n_m$ ) of the cavity (see text S1 for details), where  $k_0$  is the wave vector in vacuum,  $n_m$  is the refractive index of the medium, and  $n_c$  is the refractive index of the cavity with a radius of  $r_c$ . The validity of the first-order scattering approximation will be discussed later.

On the other hand,  $S_{ee}$ ,  $S_{mm}$ , and  $S_{em}$  are the scattering coefficient terms in the associated force components, and they are defined as:  $S_{ee} = 2(2\alpha_1\alpha_2^* + \alpha_1 + \alpha_2^*)$ ,  $S_{mm} = 2(2\beta_1\beta_2^* + \beta_1 + \beta_2^*)$ , and

$S_{em} = -2i(2\alpha_1\beta_1^* + \alpha_1 + \beta_1^*)$ . Here,  $\alpha_1$  (or  $\beta_1$ ) and  $\alpha_2$  (or  $\beta_2$ ) are, respectively, the Lorenz-Mie single sphere scattering coefficients of the electric (or magnetic) dipole and quadrupole terms (12, 13). The scattering coefficient terms depend on the size factor ( $\gamma_{np} = k_0 n_c r_{np}$ ) and the refractive index ratio ( $m_{np} = n_{np}/n_c$ ) of the NP; here,  $n_{np}$  is the refractive index of the NP with a radius of  $r_{np}$ . In Eq. 1,  $F_{ee}$  and  $F_{em}$  usually dominate in  $F_z$  for most materials (10), and their signs (i.e., positive or negative) often determine the direction of the optical force. We note that for NPs with a strong magnetic dipole resonance (e.g., Si NPs),  $F_{mm}$  can contribute to determining the sign of  $F_z$  at the resonance (14–16), but at the off-resonance wavelength, the influence of  $F_{mm}$  is insignificant, which will be shown later.

For  $r_{np}$  of 50 to 100 nm under the incident of visible or near-infrared photons [i.e., the wavelength ( $\lambda$ ) between 300 and 1000 nm], it is possible to narrow down the sign spectra of  $F_{ee}$  or  $F_{em}$ . For example, an NP with  $r_{np} = 50$  nm and  $n_{np} = 1.5$  has a negative sign for  $\mathbf{Re}(S_{ee})$  and a positive sign for  $\mathbf{Im}(S_{ee})$  (see Fig. 2, A and B). In the meantime, we find that  $\mathbf{Re}(S_{em})$  and  $\mathbf{Im}(S_{em})$  are both positive for the same particle (see Fig. 2, C and D). This restricts the signs of the modal coefficients of the incident light that can potentially achieve negative  $F_{ee}$  or  $F_{em}$  to be those shown in Table 1. In short, for  $F_{ee}$  to be negative, either “ $\mathbf{Im}(e_d e_q^*) > 0$ ” or “ $\mathbf{Re}(e_d e_q^*) < 0$ ” is the necessary condition, and for  $F_{em}$  to be negative, either “ $\mathbf{Im}(e_d m_d^*) < 0$ ” or “ $\mathbf{Re}(e_d m_d^*) < 0$ ” is needed.

When the refractive index of spherical cavity is lower than the medium ( $m_c < 1$ ), the cavity can excite unique multipole modes inside it. These internal modes can satisfy the optical conditions in Table 1 to induce OPF on the NP inside the cavity. For example, at the condition of  $n_c = 1$  and  $n_m = 1.25$  (thus,  $m_c = 0.8$ ), a spherical cavity with  $r_c = 150$  nm can lead to an optical condition of  $\mathbf{Im}(e_d e_q^*) < 0$ ,  $\mathbf{Re}(e_d e_q^*) < 0$ ,  $\mathbf{Im}(e_d m_d^*) < 0$ , and  $\mathbf{Re}(e_d m_d^*) > 0$  (see Fig. 2, A, B, D, and E) and thus OPF. We emphasize that these characteristics appear in the visible and infrared regimes. It means that the resultant  $F_{ee}$  (or  $F_{em}$ ) from a plane wave in a certain wavelength range can be negative when  $\mathbf{Im}(S_{ee})\mathbf{Re}(e_d e_q^*)$  (or  $\mathbf{Re}(S_{em})\mathbf{Im}(e_d m_d^*)$ ) dominates (see Fig. 2, E and F). We also note that this analogy can be extended to an NP with  $m_{np}$  in the range of  $0 < \mathbf{Re}(m_{np}) < 7$  and  $0 < \mathbf{Im}(m_{np}) < 7$ , which covers most real materials [i.e., Au (17), SiO<sub>2</sub> (18), or Si (19)] (see sections S2 and S3).

We then further investigate the optical force on an NP inside a dielectric spherical cavity with real material properties. Three representative NPs are considered: Au as a metal, Si as a high-index material, and SiO<sub>2</sub> as a dielectric material (see Fig. 3, A, D, and G, for optical configurations). For the spherical cavity and the surrounding medium, air ( $n_c = 1$ ) and water ( $n_m = 1.33$ ) are selected, respectively. We calculate  $F_z$  for each case using Eq. 1 for  $r_{np} = 50$  nm and  $r_c = 150$  nm. All three NPs can experience negative optical forces inside the air cavity for a certain wavelength range (see solid lines in Fig. 3, A, D, and G). We also calculate  $F_z$  for these cases using the finite-element method (FEM), which considers the full-wave interference effect. The results are in good agreement with the  $F_z$  calculated using Eq. 1, which validates the first-order scattering approximation. From these results, we can see that the negative  $F_z$  on the NPs mainly comes from the unique electromagnetic dipole and quadrupole modes inside the air cavity.

There are usually negative  $F_z$  on NPs at the wavelengths where the electric or magnetic dipole resonance is inactive. For example, a Si NP is pulled by the incident light with  $\lambda > \sim 500$  nm, where the magnetic dipole (at  $\lambda = 485$  nm) and the electric dipole (at  $\lambda = 410$  nm)

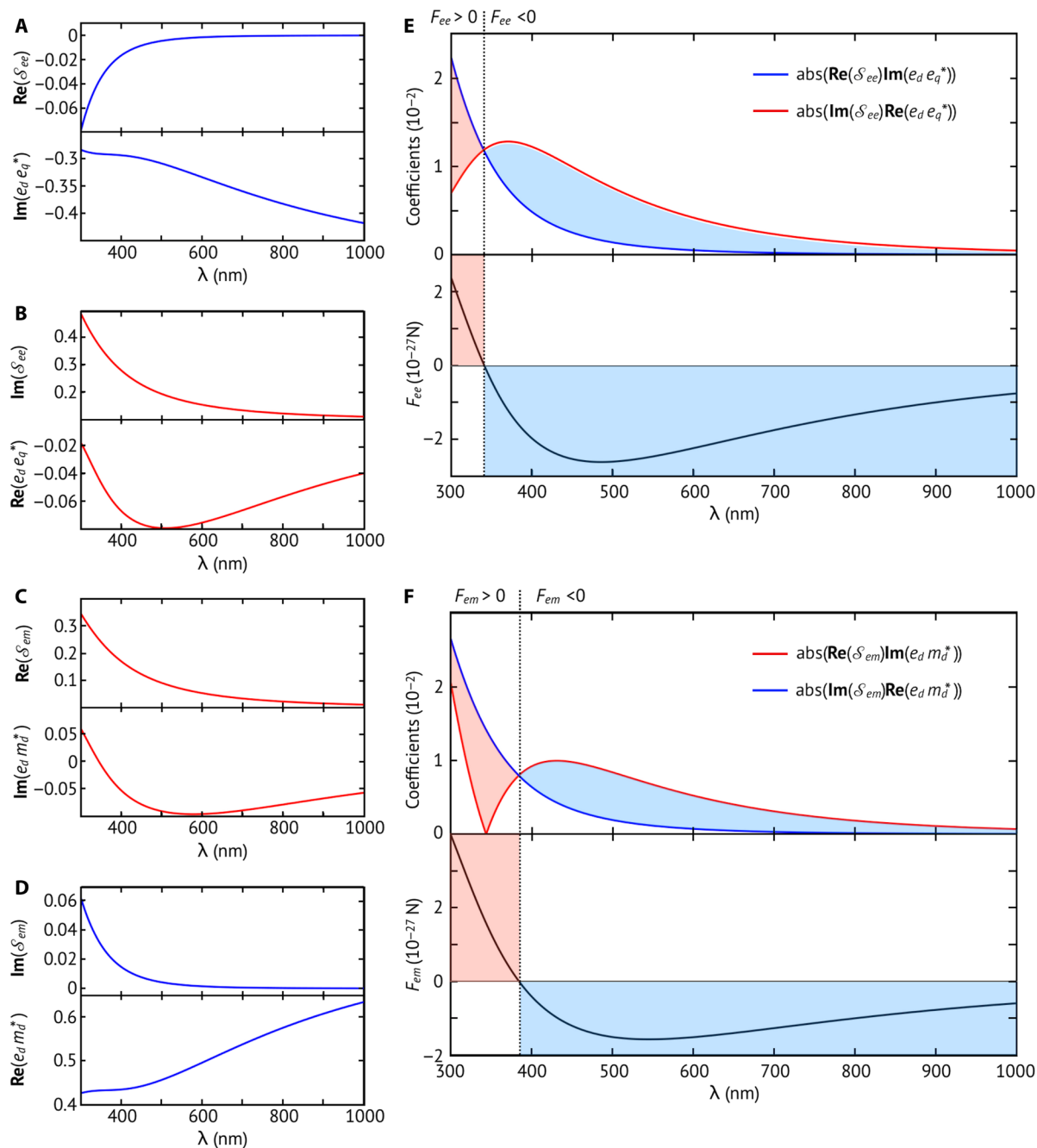


**Fig. 2. The coefficient terms and the forces on an NP ( $n_{np} = 1.5$ ) as a function of incident light wavelength ( $\lambda$ ) when the refractive index of the cavity ( $n_c = 1$ ) is lower than the medium ( $n_m = 1.25$ ). (A, B, and E) Electric dipole-quadrupole interaction components. (C, D, and F) Electric dipole-magnetic dipole interaction components. For all cases,  $|\mathbf{E}_x| = 1$ ,  $r_c = 150$  nm, and  $r_{np} = 50$  nm. In (E) and (F), the blue-shaded regions indicate that the forces are negative, and the red-shaded regions are for positive forces. Here,  $e_d$ ,  $m_d$ , and  $e_q$  are the complex amplitudes of electric dipole, magnetic dipole, and electric quadrupole modes of the incoming light to the NP, respectively;  $\mathcal{S}_{ee}$  (or  $\mathcal{S}_{em}$ ) is the scattering coefficient consisting of electric dipole and electric quadrupole (or electric dipole and magnetic dipole) of the Lorenz-Mie scattering coefficient of the NP.**

resonances are not active (Fig. 3A). At the resonance peaks, however, there is strong positive radiative pressure on the Si NP. We note that the coexistence of electric and magnetic dipoles in the visible spectrum is a well-known feature of the Si NP (14–16). Similar features are seen in the cases of Au and SiO<sub>2</sub> NPs. For the Au NP, there are positive  $F_z$  at  $300 \text{ nm} < \lambda < 580 \text{ nm}$ , with a peak around the SPR (at  $\lambda = 530 \text{ nm}$ ).

This is followed by the negative  $F_z$  at  $\lambda > 580 \text{ nm}$  as the resonance disappears. The pulling force on the SiO<sub>2</sub> NP appears at  $350 \text{ nm} < \lambda < 1000 \text{ nm}$ , above the optical resonance at  $\lambda = 140 \text{ nm}$ , which is related to the so-called photonic nano-jet phenomena (20).

We further analyze the calculated  $F_z$  with the three force components:  $F_{ee}$ ,  $F_{mm}$ , and  $F_{em}$ . As can be seen from Fig. 3 (A, D, and G)

**Table 1. Optical conditions of the incident light to achieve different signs of  $F_{ee}$  and  $F_{em}$ .** The shaded boxes highlight the optical conditions for the OPFs. Here,  $e_d$ ,  $m_d$ , and  $e_q$  are the complex amplitudes of the electric dipole, magnetic dipole, and electric quadrupole modes of the incoming light to the NP, respectively;  $S_{ee}$  (or  $S_{em}$ ) is the scattering coefficient consisting of electric dipole and electric quadrupole (or electric dipole and magnetic dipole) of the Lorenz-Mie scattering coefficient of the NP.

Electric dipole-electric quadrupole interactions		
Scattering coefficients of NP		Optical force
$\text{Re}(S_{ee}) < 0$	$\text{Im}(S_{ee}) > 0$	
Amplitudes of multipole terms of incoming light to NP $e_d$ : electric dipole, $e_q$ : electric quadrupole		
$\text{Im}(e_d e_q^*) > 0$	$\text{Re}(e_d e_q^*) < 0$	$F_{ee} < 0$
$\text{Im}(e_d e_q^*) < 0$	$\text{Re}(e_d e_q^*) < 0$	
when $ \text{Re}(S_{ee}) \text{Im}(e_d e_q^*)  <  \text{Im}(S_{ee}) \text{Re}(e_d e_q^*) $		$F_{ee} < 0$
$\text{Im}(e_d e_q^*) > 0$	$\text{Re}(e_d e_q^*) > 0$	
when $ \text{Re}(S_{ee}) \text{Im}(e_d e_q^*)  >  \text{Im}(S_{ee}) \text{Re}(e_d e_q^*) $		$F_{ee} > 0$
$\text{Im}(e_d e_q^*) < 0$	$\text{Re}(e_d e_q^*) > 0$	
Electric dipole-magnetic dipole interactions		
Scattering coefficients of NP		Optical force
$\text{Re}(S_{em}) > 0$	$\text{Im}(S_{em}) > 0$	
Amplitudes of multipole terms of incoming light to NP $e_d$ : electric dipole, $m_d$ : magnetic dipole		
$\text{Im}(e_d m_d^*) < 0$	$\text{Re}(e_d m_d^*) < 0$	$F_{em} < 0$
$\text{Im}(e_d m_d^*) > 0$	$\text{Re}(e_d m_d^*) < 0$	
when $ \text{Re}(S_{em}) \text{Im}(e_d m_d^*)  <  \text{Im}(S_{em}) \text{Re}(e_d m_d^*) $		$F_{em} < 0$
$\text{Im}(e_d m_d^*) < 0$	$\text{Re}(e_d m_d^*) > 0$	
when $ \text{Re}(S_{em}) \text{Im}(e_d m_d^*)  >  \text{Im}(S_{em}) \text{Re}(e_d m_d^*) $		$F_{em} > 0$
$\text{Im}(e_d m_d^*) > 0$	$\text{Re}(e_d m_d^*) > 0$	

(red and green dotted lines),  $F_{ee}$  and  $F_{em}$  have negative signs and dominate in each case at the wavelength range where the NP experiences OPFs. In  $F_{ee}$ , there is a competition between  $\text{Re}(S_{ee})\text{Im}(e_d e_q^*)$  and  $\text{Im}(S_{ee})\text{Re}(e_d e_q^*)$  as they can have opposite signs as discussed earlier (see Fig. 3, B, E, and H). At the wavelength where the electric or magnetic resonance is diminishing, we can see that the negative term becomes larger than the positive term, yielding a negative  $F_{ee}$ . When the electric or magnetic resonance occurs, the positive term can dominate, leading to a positive  $F_{ee}$ . These behaviors are similarly observed in  $F_{em}$  for all three NPs given that  $\text{Re}(S_{em})\text{Im}(e_d m_d^*)$  is usually negative and  $\text{Im}(S_{em}) \text{Re}(e_d m_d^*)$  tends to be positive (see Fig. 3, C, F, and I). We stress again that the OPF are due to the negative  $\text{Re}(e_d e_q^*)$  and  $\text{Im}(e_d m_d^*)$ . For  $F_{mm}$ , we see that its contribution to  $F_z$  is always much smaller than other components (see blue dots lines in Fig. 3, A, D, and G) unless the NP experiences a magnetic dipole resonance (i.e., Si NP in Fig. 3A).

Because of the OPF, the NP can deviate from the center of the cavity and moves toward the light-incoming side (i.e., the negative

$z$  direction), and this can lead to changes in the optical force. To investigate these changes, we calculate  $F_z$  as a function of the location of the NP ( $c_z$ ) on the  $z$  axis using the FEM, where  $(0, 0, c_z)$  is the center of the NP. We fix  $r_c = 150$  nm and  $r_{np} = 50$  nm, which are the same as those in Fig. 3 (A, D, and G). At  $c_z < 0$ , we find that all three types of NPs continue to experience OPFs at the wavelengths that induce the negative  $F_z$  at  $c_z = 0$ , i.e.,  $\lambda > 500$  nm for the Si NP,  $\lambda > 600$  nm for the Au NP, and  $\lambda > 450$  nm for the SiO<sub>2</sub> NP (see Fig. 3, J to L). At  $c_z > 0$ , the sign of optical force is changed to positive when the NPs are close to the opposite interior of the cavity (i.e., the positive  $z$  direction), i.e.,  $c_z = 70$  to  $80$  nm for the Si NP,  $c_z = 50$  to  $60$  nm for the Au NP, and  $c_z = 80$  to  $90$  nm for the SiO<sub>2</sub> NP. We note that as the NP approaches the interior of the cavity, the optical interference effect becomes strong, which can also contribute to determining the sign of the optical force.

To validate the above theoretical calculations, we design an experiment where a laser excites Au NPs at their SPR peak to generate a supercavity (i.e., a cavity encapsulating the NP) and at the same time provides photon streams to apply optical forces. Au NPs consisting of a silica core (radius of  $\sim 50$  nm) and an Au shell (the thickness of  $\sim 10$  nm) are selected to match the SPR with our laser frequency (800 nm). The core-shell (CS) Au NPs can create a nanobubble in the water when the illuminating light at the SPR peak ( $\lambda = 800$  nm) has a fluence greater than  $\sim 7$  mJ cm<sup>-2</sup> and ultrashort pulses ( $\sim 10$  to  $100$  fs) (21). In the fluence range of 7 to 15 mJ cm<sup>-2</sup>, the radius of the generated vapor nanobubble ( $r_b$ ) is reported to be  $\sim O(100$  nm) (21). We confirm the formation of nanobubble on the NP upon laser excitation with a pump probe-based optical scattering imaging technique (see section S4) (22, 23). Such a nanobubble acts as the lower index spherical cavity described in the above theoretical calculations. To check the sign of the optical force on the CS Au NP at  $\lambda = 800$  nm, we perform FEM simulations. For the nanobubble with  $r_b = 150$  nm, the FEM simulation predicts an OPF on the CS Au NP. We note that the SPR peak of the CS Au NP shifts to  $\sim 680$  nm in vapor from  $\sim 800$  nm in liquid water, so the photon from our laser is off-SPR after the nanobubble generation. The OPF appears when the CS Au NP is located at the light-incoming side of the cavity ( $c_z < -60$  nm) (see Fig. 4A). In the extreme of the NP contacting the interface, the negative force has a magnitude between  $3 \times 10^{-13}$  and  $9 \times 10^{-13}$  N, depending on the radius of the nanobubble (see Fig. 4B). Another factor is the optical forces on the nanobubble itself. The incident laser induces positive radiative pressure on the nanobubble with a magnitude of  $2 \times 10^{-13}$  to  $2 \times 10^{-12}$  N (see Fig. 4, A and B). The direction of force is not sensitive to either the location of the NP or the size of the bubble, and it is always positive. The optical force can promote the NP to contact the interface at the light-incoming side of the nanobubble. In the meantime, the NP subject to continued laser irradiation can maintain a high temperature of  $>700$  K (see inset in Fig. 4A). This allows the NP to instantaneously evaporate water molecules to extend the front of the nanobubble, like the Leidenfrost effect (24), and the trailing end of the nanobubble can condense back to liquid as it cools when the NP moves away from it. In such a way, the NP is always encapsulated by the nanobubble while it moves. This is the key to realize persistent optical coupling and thus long-distance movement.

We are able to experimentally capture the optical pulling of CS Au NPs using the setup shown in Fig. 4C (see Materials and Methods for more details). We observe the NP moving against the light-propagating direction for a distance of more than 100  $\mu\text{m}$  along the

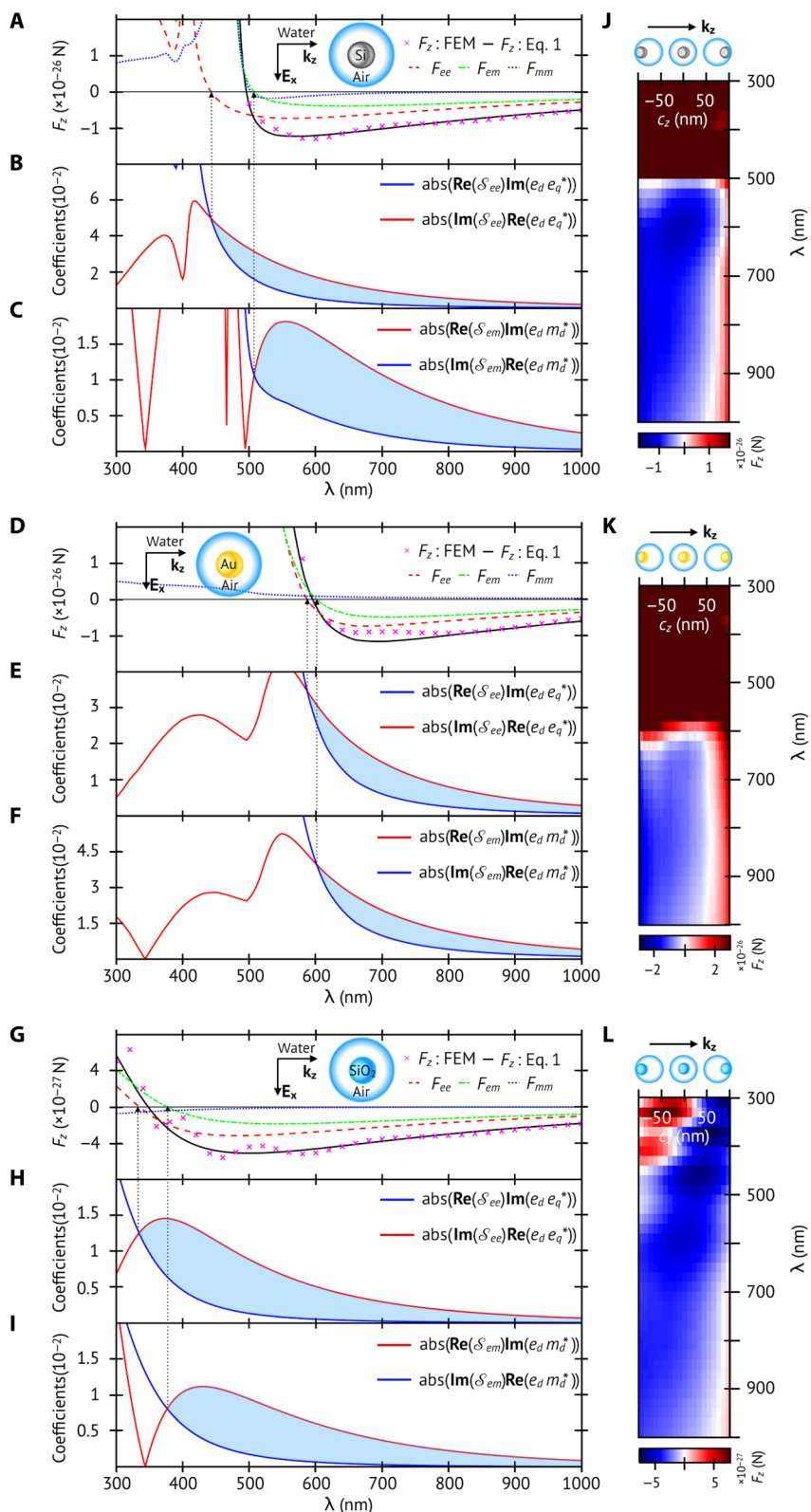


**Fig. 3. Negative optical force on the NP inside an air cavity in the medium of liquid water.** The calculated  $F_z$  on (A) Si NP, (D) Au NP, and (G) SiO<sub>2</sub> NP as a function of  $\lambda$ . For all cases,  $r_{np} = 50$  nm and  $r_c = 150$  nm. The NP and the cavity are co-centered. The insets illustrate the structure configurations. The coefficient terms as a function of  $\lambda$  for (B and C) Si NP, (E and F) Au NP, and (H and I) SiO<sub>2</sub> NP; here, the blue-shaded regions indicate that the forces are negative. (J to L) The calculated  $F_z$  from FEM as a function of  $c_z$ , where  $c_z$  is the z coordinate of the center of the NP, for (J) Si NP, (K) Au NP, and (L) SiO<sub>2</sub> NP. The structure configurations are illustrated on top of the contours. For all cases,  $|\mathbf{E}_x| = 1$ .

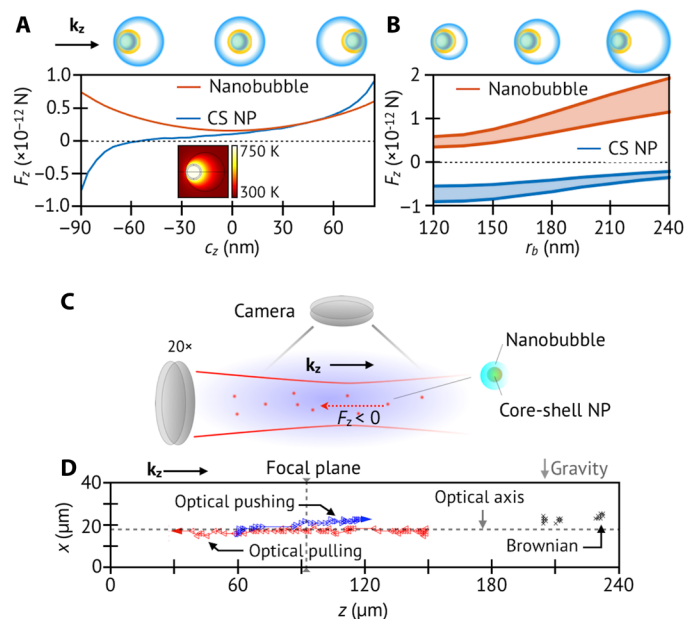


**Fig. 4. Long-distance optical pulling of Au NP.** (A) Calculated optical forces on the CS Au NP and the nanobubble as a function of the NP position in the nanobubble. The radius of nanobubble ( $r_b$ ) = 150 nm. The intensity of the incident light is set to  $12 \text{ mW } \mu\text{m}^{-2}$ . Inset: The calculated temperature profile of NP at  $c_z = -90$  nm. (B) Calculated optical forces as a function of  $r_b$  when the NP contacts the interface of the light-incoming side of the nanobubble. See the illustrated optical configuration on top of the graph. The two solid lines in each color correspond to the forces at the light intensity of  $7.2 \text{ mW } \mu\text{m}^{-2}$  (for the lower magnitude) and  $12 \text{ mW } \mu\text{m}^{-2}$  (for the higher magnitude). (C) The schematic of the experimental setup for observing the optical pulling motion of NPs. A 20x objective lens loosely focuses a femtosecond pulsed laser of  $\lambda = 800$  nm into the suspension. The focused Gaussian beam has a beam waist of  $6 \mu\text{m}$ . The fluence is  $15 \text{ mJ cm}^{-2}$  at the focal plane and  $9 \text{ mJ cm}^{-2}$  at a distance of  $120 \mu\text{m}$  away from the focal plane, which correspond to the light intensities used in (A) and (B). A high-speed camera is used to record the location of the scattered light from each NPs in the water. (D) Tracked positions of representative NPs: (red) optical pulling motion, (blue) optical pushing motion, and (black) Brownian motion. Here, the symbols in each color correspond to the positions of an NP at each time frame. The NP motions are recorded at 5000 frames  $\text{s}^{-1}$  (or frames per second).

optical axis, as shown in Fig. 4D and movie S1. In the experiment, we use a loosely focused femtosecond pulsed laser with the fluence from  $9 \text{ mJ cm}^{-2}$  (at the location of  $120 \mu\text{m}$  away from the focal plane) to  $15 \text{ mJ cm}^{-2}$  (at the focal plane). The focus is very weak, and the laser beam mimics a plane wave. The time interval between pulses is  $\sim 12$  ns, which is much shorter than the lifetime of the supercavitating nanobubbles ( $\sim 150$  ns) (21). This time scale mismatch helps to keep the nanobubble from collapsing. Since the nanobubble generation, its size, and the relative position between NP and the nanobubble are stochastic, we perform the experiment in a CS Au NP suspension with a concentration of  $\sim 10^{13} \text{ m}^{-3}$  as a statistical ensemble, hoping that some of the NPs encapsulated by the plasmonic nanobubble can have the configuration required to realize optical pulling. A high-speed camera is used to record the scattered light from NPs to track their positions as a function of time with an interval of 0.2 ms. The pulling motion is very distinguishable compared to the optical pushing or the Brownian motion (see Fig. 4D and movie S1). We pick out the pulling motions of NPs and then calculate the speed in each time interval of recording. We identify  $\sim 14$  represent-

ative cases of optical pulling motions and extract the maximum speed of NP in each case (see sections S5). The mean value of these average speeds is  $\sim 48,000 \pm 29,000 \mu\text{m s}^{-1}$ , and the maximum speed is up to  $109,000 \mu\text{m s}^{-1}$ , where the error bar represents the SD. Using the average speed of these NPs and the vapor viscosity, the Stokes' law allows us to estimate the force the NPs are experiencing. We use the viscosity of steam at 400 K ( $1.3 \times 10^{-5} \text{ kg m}^{-1} \text{ s}^{-1}$ ) (25), which corresponds to the spatial average of the calculated temperature in the nanobubble (inset in Fig. 4A). As a result, the calculated drag force is  $\sim 7.0 \times 10^{-13} \text{ N}$ , which is in good agreement with the order of magnitude of the OPF on the NP ( $3 \times 10^{-13}$  to  $9 \times 10^{-13} \text{ N}$ ) calculated from the FEM simulations (Fig. 4, A and B). This confirms that the fast-moving NPs are always encapsulated in a gaseous environment since the laser-excited NP ( $>700$  K) can instantaneously evaporate water to extend the boundary of the bubble as the NPs move.

We would like to note that there are other forces acting on the NP in the laser-irradiated suspension. These include gravity, buoyancy, optical intensity gradient force, thermal gradient force, and optical force (i.e., OPF). On the basis of the observed NP motion direction, we can rationally eliminate all but the optical force as the driving force. First, gravity and buoyancy are perpendicular to the observed fast NP moving direction and thus cannot be responsible for the movement here. If the optical intensity gradient force dominates, then we should have observed that all NPs converge to or diverge from the highest optical intensity regime (i.e., the focal plane). However, fast-moving NPs on either side of the focal plane can move in the negative direction (see sections S5). In addition, there is no trapped NPs near the focal plane, and this can be due to the fact that the numerical aperture used in our experiment is low ( $\sim 0.42$ ), and the shape of the CS NP is spherical (26, 27). Thus, optical intensity gradient force should not be the driving force. Because of the optical intensity gradient, optical heating should also induce a thermal gradient in the laser-irradiated regime, with the focal plane having the highest temperature. However, the same argument above can be applied here: the thermophoretic effect due to the temperature gradient should drive the NPs either all toward the focal plane or diverting them away from it, depending on the sign of the Soret coefficient. The above discussed NP moving directions then again eliminate the thermophoretic force as a possible driver. We also note that the NP irradiated by the laser can experience thermophoretic force due to the temperature difference across the NP itself along the laser beam axis direction (see the inset in Fig. 4A). However, the temperature difference is less than 1.0 K, which leads to the thermophoretic force of  $10^{-16}$  to  $10^{-15} \text{ N}$  (section S6). Therefore, the thermophoretic force is not important in driving the NP to move, as it is much smaller than the optical forces ( $10^{-13}$  to  $10^{-12} \text{ N}$ ; see Fig. 4B). This is reasonable because even for a Janus NP (half dielectric/half metallic) (28), which is designed to have a strong temperature difference ( $\sim 100$  K) across the NP, the thermophoretic force is only on the order of  $10^{-14} \text{ N}$ . The above analysis leaves the optical force due to photon-object momentum exchange the only possible driving force.

We also point out that not every NP exhibits long-distance movement, and many of them experience Brownian motion (Fig. 4D and movie S1). This is related to two factors: (i) the formation of nanobubbles is stochastic and depends on factors of NPs like curvature, uniformity of the Au shell layer, and surface nucleation sites (29), and thus, not every NP is guaranteed to be encapsulated by a nanobubble; and (ii) even if an NP is encapsulated by a nanobubble,

the optical force on the NP depends on the relative location of the NP in the nanobubble as shown in Fig. 4A.

In practice, the supercavitation-enabled optical pulling can be useful for nanomaterials assembly and pattern writing. The pulling force can allow one to introduce a laser from the substrate side to deposit NPs in the solution to this substrate, which would be especially useful if the solution is optically absorptive, and thus, using optical pushing force for NP deposition on the substrate is not possible. While the supercavitation strategy might not be applicable to some biological application because of the involved high temperature, as our study indicates, the optical pulling can be achieved when the spherical cavity has a refractive index lower than the medium, which may allow one to design a different cavity/medium system such as a water cavity in an oil medium (30) to realize optical pulling. This fundamental study may draw interests from different communities to realize optical pulling structures and applications based on our discovered mechanism.

## MATERIALS AND METHODS

### OPF simulation

An ideal absorbing layer (i.e., perfectly matched layer) with a thickness of 130 nm encapsulates a water sphere with a radius of 400 nm, which represents a semi-infinite medium of water. The lower cavity is located in the water medium, and the NP is placed inside the cavity. A plane wave with an electric field amplitude of unity in the  $x$  direction is used as the incident light, which propagates in the positive  $z$  direction. After solving the electromagnetic field distribution of the simulation domain using the FEM, the time-averaged Maxwell stress tensor ( $\vec{T}$ ) is integrated over the surface of the NP (or the nanobubble) to calculate optical force as:  $\oint \vec{T} \cdot \hat{n} da$ , where  $\hat{n}$  is the normal vector of the surface (10).

### Optical pulling experiment

A four-window quartz cuvette (Hellma, Sigma-Aldrich, 10 mm by 10 mm) is filled with a CS Au NPs-water suspension (Auroshell, Nanospectra Biosciences Inc.) with the concentration of  $4 \times 10^{14} \text{ m}^{-3}$ . A Ti:sapphire crystal in an optical cavity (Spectra Physics, Tsunami) emits mode-locked femtosecond laser pulses at  $\lambda = 800 \text{ nm}$ , which is collimated and linearly polarized. The repetition rate of the laser pulses is 80.7 MHz. A 20 $\times$  objective lens focuses the laser in the volume of NP-water suspension, where the fluence at the focal plane is  $15 \text{ mJ cm}^{-2}$ , with the beam waist of  $6 \mu\text{m}$  measured by a beam profiler (Thorlab BP104-UV). A high-speed camera (HX-7, NAC) records the scattered lights from the CS Au NPs in the suspension at 5000 frames  $\text{s}^{-1}$  (or frames per second). In the experiment, we open the mechanical pinhole completely to capture all possible scattered light from pulled, pushed, and Brownian NPs in the focal volume of the camera irradiated by the laser beam. Customized software in MATLAB is used to analyze the recorded images to track the pulling motion of NPs.

## SUPPLEMENTARY MATERIALS

Supplementary material for this article is available at <http://advances.sciencemag.org/cgi/content/full/6/2/eaaz3646/DC1>

## REFERENCES AND NOTES

- J. Chen, J. Ng, Z. Lin, C. T. Chan, Optical pulling force. *Nat. Photonics* **5**, 531–534 (2011).
- S. Sukhov, A. Dogariu, Negative nonconservative forces: Optical “tractor beams” for arbitrary objects. *Phys. Rev. Lett.* **107**, 203602 (2011).
- A. Novitsky, C.-W. Qiu, H. Wang, Single gradientless light beam drags particles as tractor beams. *Phys. Rev. Lett.* **107**, 203601 (2011).
- O. Brzobohatý, V. Karásek, M. Šiler, L. Chvátal, T. Čížmár, P. Zemánek, Experimental demonstration of optical transport, sorting and self-arrangement using a ‘tractor beam’. *Nat. Photonics* **7**, 123–127 (2013).
- J. Damková, L. Chvátal, J. Ježek, J. Oulehla, O. Brzobohatý, P. Zemánek, Enhancement of the ‘tractor-beam’ pulling force on an optically bound structure. *Light Sci. Appl.* **7**, 17135 (2018).
- X. Li, J. Chen, Z. Lin, J. Ng, Optical pulling at macroscopic distances. *Sci. Adv.* **5**, eaau7814 (2019).
- V. Kajorndejnukul, W. Ding, S. Sukhov, C.-W. Qiu, A. Dogariu, Linear momentum increase and negative optical forces at dielectric interface. *Nat. Photonics* **7**, 787–790 (2013).
- A. Mirzahi, Y. Fainman, Negative radiation pressure on gain medium structures. *Opt. Lett.* **35**, 3405–3407 (2010).
- K. J. Webb, Shivanand, Negative electromagnetic plane-wave force in gain media. *Phys. Rev. E Stat. Nonlin. Soft Matter Phys.* **84**, 057602 (2011).
- G. Guo, T. Feng, Y. Xu, Tunable optical pulling force mediated by resonant electromagnetic coupling. *Opt. Lett.* **43**, 4961–4964 (2018).
- J. Kesava, P. C. Chaumet, T. N. Langtry, A. Rahmani, Optical binding of electrically small magnetodielectric particles. *J. Nanophotonics* **4**, 041583 (2010).
- A. Salandrino, S. Fardad, D. N. Christodoulides, Generalized Mie theory of optical forces. *J. Opt. Soc. Am. B* **29**, 855–866 (2012).
- D. W. Mackowski, Analysis of radiative scattering for multiple sphere configurations. *Proc. R. Soc. Lond. A* **433**, 599–614 (1997).
- Y. Kivshar, A. Miroshnichenko, Meta-optics with Mie resonances. *Opt. Photonics News* **28**, 24–31 (2017).
- S. Kruk, Y. Kivshar, Functional meta-optics and nanophotonics governed by Mie resonances. *ACS Photonics* **4**, 2638–2649 (2017).
- A. B. Evlyukhin, S. M. Novikov, U. Zywietz, R. L. Eriksen, C. Reinhardt, S. I. Bozhevolnyi, B. N. Chichkov, Demonstration of magnetic dipole resonances of dielectric nanospheres in the visible region. *Nano Lett.* **12**, 3749–3755 (2012).
- P. B. Johnson, R. W. Christy, Optical constants of the noble metals. *Phys. Rev. B* **6**, 4370–4379 (1972).
- L. V. Rodríguez-de Marcos, J. I. Larruquert, J. A. Méndez, J. A. Aznárez, Self-consistent optical constants of SiO<sub>2</sub> and Ta<sub>2</sub>O<sub>5</sub> films. *Opt. Mater. Express* **6**, 3622–3637 (2016).
- C. Schinke, P. Christian Peest, J. Schmidt, R. Brendel, K. Bothe, M. R. Vogt, I. Kröger, S. Winter, A. Schirmacher, S. Lim, H. T. Nguyen, D. MacDonald, Uncertainty analysis for the coefficient of band-to-band absorption of crystalline silicon. *AIP Adv.* **5**, 067168 (2015).
- B. S. Luk'yanchuk, R. Paniagua-Domínguez, I. Minin, O. Minin, Z. Wang, Refractive index less than two: Photonic nanojets yesterday, today and tomorrow [Invited]. *Opt. Mater. Express* **7**, 1820–1847 (2017).
- R. Lachaine, C. Boutopoulos, P.-Y. Lajoie, É. Boulais, M. Meunier, Rational design of plasmonic nanoparticles for enhanced cavitation and cell perforation. *Nano Lett.* **16**, 3187–3194 (2016).
- E. Lukianova-Hleb, Y. Hu, L. Latterini, L. Tarpani, S. Lee, R. A. Drezek, J. H. Hafner, D. O. Lapotko, Plasmonic nanobubbles as transient vapor nanobubbles generated around plasmonic nanoparticles. *ACS Nano* **4**, 2109–2123 (2010).
- R. Lachaine, E. Boulais, E. Bourbeau, M. Meunier, Effect of pulse duration on plasmonic enhanced ultrafast laser-induced bubble generation in water. *Appl. Phys. A* **112**, 119–122 (2013).
- I. U. Vakarelski, E. Klaseboer, A. Jetly, M. M. Mansoor, A. A. Aguirre-Pablo, D. Y. C. Chan, S. T. Thoroddsen, Self-determined shapes and velocities of giant near-zero drag gas cavities. *Sci. Adv.* **3**, e1701558 (2017).
- J. Kestin, H. E. Wang, The viscosity of superheated steam up to 270° C. *Phys. Ther.* **26**, 575–584 (1960).
- R. Saija, P. Denti, F. Borghese, O. M. Maragò, M. A. Iati, Optical trapping calculations for metal nanoparticles. Comparison with experimental data for Au and Ag spheres. *Opt. Express* **17**, 10231–10241 (2009).
- O. Brzobohatý, M. Šiler, J. Trojek, L. Chvátal, V. Karásek, A. Paták, Z. Pokorná, F. Mika, P. Zemánek, Three-dimensional optical trapping of a plasmonic nanoparticle using low numerical aperture optical tweezers. *Sci. Rep.* **5**, 8106 (2015).
- M. Xuan, Z. Wu, J. Shao, L. Dai, T. Si, Q. He, Near infrared light-powered Janus mesoporous silica nanoparticle motors. *J. Am. Chem. Soc.* **138**, 6492–6497 (2016).
- C. Li, Z. Wang, P.-I. Wang, Y. Peles, N. Koratkar, G. P. Peterson, Nanostructured copper interfaces for enhanced boiling. *Small* **4**, 1084–1088 (2008).
- Z. Pan, Y. Men, S. Senapati, H.-C. Chang, Immersed AC electrospray (iACE) for monodispersed aqueous droplet generation. *Biomicrofluidics* **12**, 044113 (2018).

### Acknowledgments

**Funding:** This work is supported by the National Science Foundation (1706039) and the Center for the Advancement of Science in Space (CASIS GA-2018-268). **Author**

**contributions:** E.L. and T.L. designed the experiments. E.L. set up and performed the experiments and performed optical analysis and simulations. E.L. and T.L. discussed the results and wrote the manuscript. **Competing interests:** The authors declare that they have no competing interests. **Data and materials availability:** All data needed to evaluate the conclusions in the paper are present in the paper and/or the Supplementary Materials. Additional data related to this paper may be requested from the authors.

Submitted 3 September 2019

Accepted 16 March 2020

Published 20 May 2020

10.1126/sciadv.aaz3646

**Citation:** E. Lee, T. Luo, Long-distance optical pulling of nanoparticle in a low index cavity using a single plane wave. *Sci. Adv.* **6**, eaaz3646 (2020).

## Long-distance optical pulling of nanoparticle in a low index cavity using a single plane wave

E. Lee and T. Luo

*Sci Adv* **6** (21), eaaz3646.  
DOI: 10.1126/sciadv.aaz3646

**ARTICLE TOOLS** <http://advances.sciencemag.org/content/6/21/eaaz3646>

**SUPPLEMENTARY MATERIALS** <http://advances.sciencemag.org/content/suppl/2020/05/18/6.21.eaaz3646.DC1>

**REFERENCES** This article cites 30 articles, 2 of which you can access for free  
<http://advances.sciencemag.org/content/6/21/eaaz3646#BIBL>

**PERMISSIONS** <http://www.sciencemag.org/help/reprints-and-permissions>

Use of this article is subject to the [Terms of Service](#)

---

*Science Advances* (ISSN 2375-2548) is published by the American Association for the Advancement of Science, 1200 New York Avenue NW, Washington, DC 20005. The title *Science Advances* is a registered trademark of AAAS.

Copyright © 2020 The Authors, some rights reserved; exclusive licensee American Association for the Advancement of Science. No claim to original U.S. Government Works. Distributed under a Creative Commons Attribution NonCommercial License 4.0 (CC BY-NC).